Theor Chem Account (2007) 118:665–671
DOI 10.1007/s00214-007-0355-x

REGULAR ARTICLE

Transition metal impurities in wide gap materials: are the electronic properties well described through the ligand field theory?

M. Moreno · J. M. García-Lastra · M. T. Barriuso · J. A. Aramburu

Received: 13 February 2007 / Accepted: 29 April 2007 / Published online: 12 June 2007

Abstract In the traditional ligand field theory the electronic properties due to a transition metal (TM) impurity, M, in an insulator are explained only in terms of the MX_N complex formed with the N nearest anions. This work is aimed at emphasizing the role played by the electrostatic potential, $V_R(\mathbf{r})$, exerted by the rest of lattice ions upon the localized electrons of the TM complex. This potential, neglected in the traditional ligand field theory, is shown to play a key role when comparing the electronic properties of the same TM complex but embedded in two lattices which are not isomorphous even if both are cubic. As a relevant example it is shown that the different 10 Dq values exhibited by CrF_6^{3-} in the normal perovskite $KMgF_3$(10 Dq = 14, 100 cm^{-1}) and in the inverted perovskite $BaLiF_3$(10 Dq = 16, 720 cm^{-1}) can hardly be understood only through a distinct Cr^{3+}–F^- distance. In contrast such a difference is shown to come mainly from the different shape of $V_R(\mathbf{r})$ in these two cubic lattices. The importance of this internal electric field is pointed out to grow when comparing two host lattices with the same ligand and coordination number but very different symmetry. This situation is found in the case of ruby (Al_2O_3 : Cr^{3+}) and emerald ($Be_3Si_6Al_2O_{18}$: Cr^{3+}) where $V_R(\mathbf{r})$ is behind the different colours exhibited by such gemstones. For the sake of clarity a brief discussion on the foundations of the ligand field theory is reported in the present work as well.

Contribution to the Serafin Fraga Memorial Issue.

M. Moreno · J. A. Aramburu (✉)
Departamento de Ciencias de la Tierra y Física de la Materia Condensada, Universidad de Cantabria, 39005 Santander, Spain
e-mail: aramburj@unican.es

J. M. García-Lastra · M. T. Barriuso
Departamento de Física Moderna, Universidad de Cantabria, 39005 Santander, Spain

1 Introduction

Since the seminal work by A. Werner it is known that the colour exhibited by compounds like $CoCl_3(NH_3)_6$ can be understood to a good extent considering only the $Co(NH_3)_6^{3+}$ complex molecule [1]. In the same vein the electronic properties due to a transition metal impurity, M, in an insulating lattice are usually explained *only* in terms of the MX_N complex formed with the N nearest ions [2–6]. This idea, which is behind the traditional ligand field theory, actually implies an enormous simplification. In fact, a problem in the realm of solid state physics is reduced to a molecular problem involving only few atoms.

In the spirit of the ligand field theory (LFT) the properties of a MX_N molecule can be modified either by applying a hydrostatic pressure or by changing the host lattice where the complex is embedded. Both actions lead to a modification of the equilibrium M–X distance, R, which in turn produces variations on excitation energies or spin Hamiltonian parameters. This distance is in general different to that corresponding to the perfect lattice, henceforth designated by R_0. These ideas have been well verified looking at optical and electron paramagnetic resonance (EPR) spectra of Mn^{2+}, Ni^{2+} and Fe^{3+} impurities placed in the series of *normal* cubic fluoroperovskites [7]. For instance the excitation spectrum of $RbCdF_3$: Mn^{2+} is not the same as that for $KMgF_3$: Mn^{2+} and the differences between them have reasonably been ascribed to the different equilibrium Mn^{2+}–F^- distance in $RbCdF_3$ and $KMgF_3$ host lattices [8]. Such a difference ultimately reflects the distinct lattice parameter, a, in $RbCdF_3$($a = 2R_0 = 4.3$ Å) and $KMgF_3$($a = 4.0$ Å). A similar situation to this one has been found for Cr^{3+} in cubic elpasolites [9].

Despite these well-established facts a puzzling issue comes out when comparing the optical spectra of the same

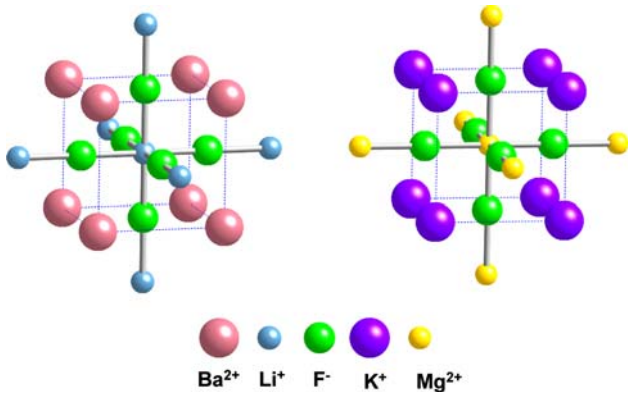

Fig. 1 Twenty-one atom clusters used in the calculations of the inverse $BaLiF_3$ (*left*) and normal $KMgF_3$ (*right*) perovskite structures. Unit cells are marked with *dashed lines*. The lattice constant a is thus equal to $2\,R_0$. Similar clusters were used for the calculations of the corresponding Ni^{2+} impurity centers but replacing the central ion (Li^+ in $BaLiF_3$ and Mg^{2+} in $KMgF_3$) by Ni^{2+}

impurity placed in two lattices which are both cubic but *not isomorphous*. This is the case of $KMgF_3$ and $BaLiF_3$ whose structure is displayed in Fig. 1. The first compound exhibits the normal perovskite structure [10] where the divalent cation is surrounded by an octahedron of F^- ions. In contrast, $BaLiF_3$ shows the so-called inverse perovskite structure [11] where it is the monovalent cation which is surrounded by an octahedron of fluorine ions. In $KMgF_3$ 3d cations like Cr^{3+}, Ni^{2+} or Mn^{2+} enter the Mg^{2+} site while in $BaLiF_3$ they occupy the Li^+ place as unequivocally demonstrated by EPR and electron nuclear double resonance (ENDOR) techniques [12–15]. This fact reflects the closeness of ionic radii of Mg^{2+} and Li^+ which in turn makes that the Mg^{2+}–F^- distance in $KMgF_3$ and the Li^+–F^- distance in $BaLiF_3$ are the same within 0.3% [10,11]. For this reason it can be expected within the traditional LFT that an impurity like Cr^{3+} gives rise to the same optical absorption spectrum when placed either in $KMgF_3$ or in the $BaLiF_3$ host lattice. This statement is, however, not confirmed by experimental data. For instance, the value of the ${}^4A_{2g}(t_{2g}^3) \rightarrow {}^4T_{2g}(t_{2g}^2 e_g)$ transition energy (equal to the value of the cubic field splitting parameter termed as 10 Dq) is found to be equal to 14, 100 cm^{-1} for $KMgF_3 : Cr^{3+}$ while $10\,Dq = 16,720\,cm^{-1}$ measured for $BaLiF_3 : Cr^{3+}$ is 18.6% higher [12,13]. A similar situation holds [15] when comparing the experimental 10 Dq values of $KMgF_3 : B^{2+}$ and $BaLiF_3 : B^{2+}$ where B = Mn or Ni. It is worth noting here that while for impurities like Mn^{2+} or Ni^{2+} in $KMgF_3$ no charge compensation is required, this is no longer true for Cr^{3+}. Nevertheless, similar to what happens [15–17] with Fe^{3+} in $KMgF_3$ or Ni^{2+} in $BaLiF_3$, a cubic centre involving a *remote* charge compensation is formed in $KMgF_3 : Cr^{3+}$ [12]. In contrast, in $BaLiF_3 : Cr^{3+}$ EPR data reveal [13] that all centres formed have a local trigonal symmetry ascribed to a compensating Ba^{2+} vacancy. This perturbation is, however, not seen in the broad optical absorption spectrum.

The present work is aimed at exploring this puzzling situation which can hardly be understood within the traditional LFT. It is shown along this work that this problem can easily be solved once the electric field exerted by other ions of lattice upon the active electrons in the complex is taken into account. This key point, *not considered* in the traditional LFT, is also pointed out to be behind the different colour exhibited by ruby and emerald.

For the sake of clarity a discussion on the basis of the LFT is first given in Sect. 2. A brief account of calculations carried out on $KMgF_3 : Cr^{3+}$ and $BaLiF_3 : Cr^{3+}$ is reported in Sect. 3 while main results are collected in Sect. 4. For the sake of completeness a recall of main results recently reached on ruby and emerald [18,19] are also reported at the end of Sect. 4.

2 Impurities in insulators: grounds of the ligand field theory

Good insulating materials like KF, $KMgF_3$ or Al_2O_3 can be described in terms of ions possessing a closed shell structure. In KF or $KMgF_3$ the valence electrons of F^- ions have the smallest binding energy. For instance, in KF the binding energy of a $2p(F^-)$ electron is 12 eV while that corresponding to a $3p(K^+)$ one is 24 eV [20]. The difference between these values and those corresponding to $2p(F^-)$ and $3p(K^+)$ of *free* F^- and K^+ ions (equal to 3.4 and 32 eV, respectively) is partially due to the Madelung potential raising (decreasing) the energy of electronic levels of cations (anions). Similarly, the binding energy of $2p(F^-)$, $3p(K^+)$ and $2p(Mg^{2+})$ levels in $KMgF_3$ should be not far from 14, 22 and 56 eV, respectively, taking 78.5 eV as the ionization potential for Mg^{2+} [21].

Let us designate by $\varphi_{n,\gamma}(\gamma = 1, 2 \text{ or } 3)$ the three p orbitals associated with the $n F^-$ ion in the lattice. The ground state of KF can be built by a Slater determinant involving filled *localized* orbitals like $\varphi_{n,\gamma}$. Alternatively, a tight-binding or molecular orbital scheme can be used to depict such a ground state. In this framework, based on the Hartree–Fock approximation, each electron occupies however *delocalized* one-electron orbitals, $\psi_{\mathbf{k}}$. In particular, the $\psi_{\mathbf{k}}$ orbitals of the valence band are formed as linear combinations of atomic $\varphi_{n,\gamma}$ orbitals

$$\psi_{\mathbf{k}} = \sum c_{n,\gamma}^{\mathbf{k}} \varphi_{n,\gamma} \quad c_{n,\gamma}^{\mathbf{k}} \propto e^{i\mathbf{k}\boldsymbol{\tau}_n} \tag{1}$$

where $\{\boldsymbol{\tau}_n\}$ describes the anion sublattice of KF and the *delocalized* $\psi_{\mathbf{k}}$ orbitals are properly normalized .

It is worth emphasizing here that although the two descriptions involving either localized or delocalized one-electron orbitals are *apparently* very different they give rise, however,

to the same total wavefunction when *closed shell* species are involved. An illustrative example for this aim is provided by simple H_2 and He_2 molecules. While for H_2 the total wavefunction built through the molecular orbital scheme is clearly different from that obtained through localized orbitals (Heitler–London description) both schemes lead to the same total wavefunction for He_2 [22]. This fact emphasizes that the concept of localization in solids is not a property of individual electrons but of the total wavefunction as a whole, a key point emphasized by Kohn [23].

In $KMgF_3$, Mg^{2+} ions can be replaced by transition metal impurities with an open shell structure like Mn^{2+}, Ni^{2+}or Cr^{3+}. In these cases it turns out that the energy of 3d orbitals is comparable to that of $2p(F^-)$ orbitals. This fact mainly comes again from the influence of the Madelung potential raising the energy of electronic levels of the cation impurity [7]. Due to this circumstance a covalent bonding is established between the open shell impurity and the nearest anions or ligands giving rise to a transfer of electronic charge from ligands to the impurity. It should be noticed that this global transfer *also* means that the unpaired 3d electrons lying initially on the impurity spend some time on the ligands. In general, close cations to the impurity do not participate in any covalent bonding. An exception to this rule appears, however, when the valence levels of the impurity lie close to the bottom of the host lattice conduction band. This rare situation appears, for instance, in KCl containing silver neutral atoms at cationic positions [24].

Leaving aside this special circumstance, covalent bonding takes place only between the transition metal impurity and ligands while the rest of lattice ions are not altered. This statement means that active electrons coming from the M impurity are *localized* in the MX_N complex. According to this fact it has widely been assumed that electronic properties related to the M impurity can only be modified at $T = 0\,K$ by changing the M–X distance.

It should be emphasized now that a MX_N complex is never isolated but embedded in a lattice made of ions. Let us assume in a first step that the rest of ions lying outside the complex display a spherical symmetry. In such a case the electrostatic potential, $V_R(\mathbf{r})$, exerted by the rest of lattice ions upon the localized electrons of the MX_N complex is rigorously constant and then can be neglected for calculating optical transitions or EPR parameters. Although a spherical symmetry is never reached in a crystal it has been shown that for a normal perovskite lattice $V_R(\mathbf{r})$ is nearly flat [7,25] and thus the electronic properties can be accounted for considering only the MX_N complex at the right equilibrium distance. It is worth noting now that this result has been taken as general in the framework of LFT. For this reason the influence of $V_R(\mathbf{r})$ for explaining the different properties exhibited by the same complex embedded in two *not isomorphous* insulating lattices has usually been neglected. Despite this fact, the different $V_R(\mathbf{r})$ potential in the cubic elpasolite lattice K_2NaCrF_6 and in CrF_3 (space group D_{3d}^6) was stressed [26–29] to be behind the distinct 10 Dq values measured for these two chromium *compounds*. In the same vein it has been pointed out that the experimental charge transfer spectra of $CuX_4(NH_3)_2^{2-}$ complexes embedded in NH_4X lattices (X = Cl, Br) cannot be understood without considering the deep influence of the tetragonal $V_R(\mathbf{r})$ potential associated with the *interstitial* position of the Cu^{2+} impurity in these lattices with CsCl structure [29].

A main goal of this work is to show that the role of $V_R(\mathbf{r})$ cannot be ignored when comparing the properties of an impurity placed in two lattices with the same ligand and coordination number *even* if such lattices are *both* cubic.

3 Computational details

Calculations have been performed in the framework of the density functional theory (DFT) by means of the Amsterdam density functional (ADF) code [31]. All results shown in this work on Cr^{3+}-doped $KMgF_3$ and $BaLiF_3$ lattices have been performed on $CrF_6K_8Mg_6^{17+}$ and $CrF_6Ba_8Li_6^{19+}$ clusters (Fig. 1), respectively. It has been verified that active electrons are lying essentially in the CrF_6^{3-} complex. A similar conclusion was obtained for Mn^{2+} impurities in cubic fluoroperovskites by means of DFT calculations on 21 atom clusters, leading to R values very close to experimental ones [32, 33]. The exchange-correlation energy was computed according to the generalized gradient approximation (GGA) by means of Becke–Perdew functional [34,35]. All atoms were described through basis sets of TZP quality (triple-ζ Slater-type orbitals plus one polarization function) given in the program data base and the core electrons ($1s$–$3p$ for Cr and K, $1s$ for F and Li, $1s$–$2p$ for Mg, and $1s$–$4d$ for Ba) were kept frozen. The electrostatic potential from the rest of the lattice ions was generated [36] by means of 224 point charges with values previously fitted to reproduce the electric field corresponding to the infinite system. 10 Dq parameters were calculated through an approximate average-of-configuration procedure [37] in which each d-orbital was partially occupied with 8/5 electrons. In this situation 10 Dq values can simply be taken as the energy difference between e_g and t_{2g} one-electron levels.

4 Results and discussion

4.1 Influence of $V_R(\mathbf{r})$ on Cr^{3+}-doped $KMgF_3$ and $BaLiF_3$

For testing the reliability of present calculations $MgF_6K_8Mg_6^{16+}$ and $LiF_6Ba_8Li_6^{16+}$ clusters related to pure $KMgF_3$ and $BaLiF_3$ host lattices, respectively, have first been considered. If only the distances between the central cation

Table 1 Calculated values of the equilibrium Cr^{3+}–F^- distance, R, and 10 Dq parameter obtained at that distance for $KMgF_3 : Cr^{3+}$ and $BaLiF_3 : Cr^{3+}$ using 21 atom clusters (see Fig. 1).

Lattice	R_0 (experimental)	R_0 (calculated)	R (calculated)	10 Dq (experimental)	10 Dq (calculated)
$KMgF_3$	1.993	2.019	1.922	14100	15261
$BaLiF_3$	1.998	2.040	1.908	16720	17285

Experimental [17–19] and calculated values of R_0 distances corresponding to the perfect lattices are also included. Experimental 10 Dq values for both systems [11] are given for comparison. R and R_0 are given in Å and 10 Dq values in cm^{-1} units

and the nearest anions are optimized in the geometry calculations (keeping the other ions of the clusters at their host lattice positions) it is obtained $R_0 = 2.015$ Å for $KMgF_3$ and $R_0 = 2.040$ Å for $BaLiF_3$ (Table 1). With respect to experimental values given in Table 1 these calculated figures mean a deviation of 1.1% for $KMgF_3$ and 2% for $BaLiF_3$.

When Cr^{3+} enters $KMgF_3$ at the Mg^{2+} site or $BaLiF_3$ at the Li^+ site the calculated equilibrium Cr^{3+}–F^- distance, R, is found to be close to 1.90 Å. This result is reasonable considering that the average Cr^{3+}–F^- distance of pure compounds involving octahedral or distorted octahedral CrF_6^{3-} units is always near to such a figure. Along this line the measured Cr^{3+}–F^- distance for K_3CrF_6 is 1.90 Å while that calculated using a 21 atoms cluster is found to lie in the 1.86–1.88 Å domain [38].

Results collected in Table 1 indicate that the calculated R values for $KMgF_3 : Cr^{3+}$ and $BaLiF_3 : Cr^{3+}$ are identical within 0.7%. For Cr^{3+} impurities in cubic elpasolite lattices the observed variation of the cubic field splitting parameter, 10 Dq, under hydrostatic or chemical pressures has been shown [7,9,38] to reflect the changes of R through the law

$$10\,\mathrm{Dq} = C\,R^{-n} \tag{2}$$

where C is a constant and the exponent n is usually found to lie in the 4–6 range. A similar situation has been found [7] for impurities like Mn^{2+} and Ni^{2+} in cubic fluoroperovskites. The actual origin of the high sensitivity of 10 Dq to R changes has already been discussed [7,39].

If the law given by Eq. (2) is also valid for comparing Cr^{3+} in the normal and the inverse perovskite one would expect a difference between the 10 Dq values $BaLiF_3 : Cr^{3+}$ and $KMgF_3 : Cr^{3+}$ around 500 cm^{-1}. However, both the experimental and calculated values of such a difference (Table 1) are around 2, 000 cm^{-1} and thus about four times higher than the figure derived assuming that Eq. (2) is valid.

This puzzling situation can be cleared up taking into account the form of the $V_R(\mathbf{r})$ potential in both the normal and inverted perovskite structures. In Fig. 2 the potential energy, $(-e)V_R(\mathbf{r})$, felt by an electron along a principal direction for both $KMgF_3$ and $BaLiF_3$ lattices, is portrayed. It can first be noted that the shape of $(-e)V_R(\mathbf{r})$ along a ⟨100⟩ direction of the normal perovskite structure is very flat indeed though

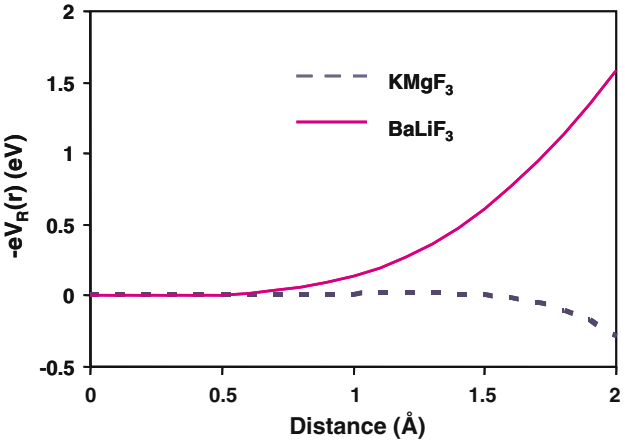

Fig. 2 Electrostatic potential, $V_R(\mathbf{r})$, of the rest of lattice ions on a NiF_6^{4-} complex depicted along ⟨100⟩ type directions for $BaLiF_3$ (*solid line*) and $KMgF_3$ (*dashed line*)

it decreases slightly in the ligand region. By contrast, in the inverted perovskite lattice $(-e)V_R(\mathbf{r})$ is found to be less flat than for the normal one and *increases* in the ligand zone. The results depicted in Fig. 2 are not unreasonable when compared to the form displayed by $V_R(\mathbf{r})$ in different cubic lattices. For instance, it has been found that in the ligand region the behaviour of $V_R(\mathbf{r})$ for a NaCl lattice is not the same as that for a normal perovskite structure [7].

As in an octahedral unit like CrF_6^{3-} only the antibonding e_g electrons have σ bonding with ligands the effects of the $V_R(\mathbf{r})$ potential are expected to be bigger on $e_g(\sim x^2-y^2, 3z^2-r^2)$ than on $t_{2g}(\sim xy, xz, yz)$ orbitals. Taking into account that for the inverted perovskite structure $(-e)V_R(\mathbf{r})$ increases the energy of the electronic density placed in the ligand region, this fact raises the $e_g(\sim x^2-y^2, 3z^2-r^2)$ level and thus the 10 Dq value. In contrast, according to Fig. 2 the effects of $V_R(\mathbf{r})$ in the normal perovskite lattice should be smaller than for the inverted one and produce a decrement of 10 Dq. This reasoning is thus able to explain albeit qualitatively why there can be a difference in the 10 Dq values for $KMgF_3 : Cr^{3+}$ and $BaLiF_3 : Cr^{3+}$ *even* if R is the same in both centres.

To put it other way let us consider in a first step an octahedral complex like CrF_6^{3-} in vacuo. The corresponding energy difference between $e_g(\sim x^2-y^2, 3z^2-r^2)$ and $t_{2g}(\sim xy,$

xz, yz) orbitals will be denoted as $[10\,\mathrm{Dq(R)}]_v$. When the complex is inserted in a lattice (even if the host lattice is cubic) there is a *supplementary* contribution to 10 Dq [18,19] coming from the electrostatic potential of the rest of lattice ions upon the electrons in the complex, Δ_R. So the actual 10 Dq value can be written as

$$10\,\mathrm{Dq} = [10\,\mathrm{Dq}(R)]_v + \Delta_R \tag{3}$$

According to the preceding discussion the positive value of Δ_R for the inverted perovskite is the main responsible for the higher 10 Dq value of $BaLiF_3 : Cr^{3+}$ when compared to that for $KMgF_3 : Cr^{3+}$ calculated at the same distance.

To gain a further insight on this issue it is now necessary to understand the different behaviour of $V_R(\mathbf{r})$ in the two types of cubic lattices. The dominant contribution to 10 Dq, $[10\,\mathrm{Dq}(R)]_v$, arises from the different chemical bonding in the σe_g level and in the πt_{2g} level of an octahedral complex [2,7,25]. In contrast, the contribution Δ_R is the result of the electrostatic interaction of outer ions with the active electrons in the complex [18,19]. For this reason Δ_R can be modelled in a first approach through the crystal field theory [15]. Each shell of ions lying outside the complex gives a contribution to Δ_R which depends on the distance, R_s to the impurity. Bearing in mind that in a cubic crystal that contribution [2–5] depends on R_s^{-5}, main differences between the shape of $V_R(\mathbf{r})$ for the normal and inverted perovskite lattices (Fig. 2) can reasonably be understood considering only the first two shells of ions lying outside the CrF_6^{3-} complex. In $KMgF_3$ (Fig. 1) the first shell is composed of eight monovalent K^+ ions displaying a cube and lying at a distance $\sqrt{3}R_0$ from the impurity . This gives rise to a positive contribution to 10 Dq favouring to locate the e_g level above the t_{2g} one. In contrast, the second shell in $KMgF_3$ is made of an octahedron of divalent Mg^{2+} ions placed at a distance $2R_0$ from the impurity thus giving rise to a negative contribution to 10 Dq. Although the latter ions are placed a little further than the former ones they are doubly charged in comparison to K^+ ions. This makes that the absolute value of the second shell contributions to 10 Dq is only a little higher than that coming from the first shell. Although this reasoning explains albeit qualitatively why $V_R(\mathbf{r})$ in the normal perovskite lattice is very flat a quantitative discussion on this issue is given in Ref. [15].

According to this view it can now be understood that a quite different situation holds for the inverse perovskite $BaLiF_3$ where the divalent Ba^{2+} ions are in the first and not in the second shell. This leads to a dominant positive contribution to 10 Dq (as shown in Fig. 2) not compensated by six Li^+ ions placed in the second shell.

4.2 Importance of $V_R(\mathbf{r})$ for $Al_2O_3 : Cr^{3+}$ and $Be_3Si_6Al_2O_{18} : Cr^{3+}$

In accordance with the analysis of the preceding section it can be expected that the importance of $V_R(\mathbf{r})$ can grow when comparing two host lattices imposing a *different* local symmetry to the substitutional impurity. A good example for this purpose is given by ruby ($Al_2O_3 : Cr^{3+}$) and emerald ($Be_3Si_6Al_2O_{18} : Cr^{3+}$) [6,40–42]. So, while for emerald the local symmetry is D_3 it is C_3 for ruby thus implying only one symmetry axis present in the later case. In agreement with this different local symmetry recent Extended X-Ray Absorption Fine Structure (EXAFS) measurements [42–44] reveal that in the case of emerald the six Cr^{3+}–O^{2-} bonds involved in the CrO_6^{9-} complex have all the same length $R = 1.97$ Å. In contrast, in ruby three O^{2-} ligands are found to be placed at $R_s = 1.92$ Å while the three other ligands are at $R_l = 2.02$ Å. Despite the existence of this small distortion in ruby the average metal–ligand distance R(ruby) = 1.97 Å coincides with that for emerald within the experimental uncertainty (±0.01 Å) involved in the EXAFS measurements [42]. Therefore, if the average Cr^{3+}–O^{2-} distance is the same for both gemstones and 10 Dq only depends on such a distance one should expect that the center of the gravity of the ${}^4A_{2g}(t_{2g}^3) \rightarrow {}^4T_{2g}(t_{2g}^2 e_g)$ transition energy would be the same for ruby and emerald. However, this statement is known to be wrong because the ${}^4A_{2g} \rightarrow {}^4T_{2g}$ absorption band is peaked at $18,070$ and $16,130\,\mathrm{cm}^{-1}$ for ruby and emerald [6,40–42], respectively, thus being responsible for the red colour of ruby and the green colour of emerald. Historically [6,40,45], this remarkable difference in colour was often explained *assuming* that 10 Dq only depends on the average Cr^{3+}–O^{2-} distance, being this distance ~ 0.05 Å smaller for ruby than for emerald. However, the referred EXAFS results [42–44] have unambiguously demonstrated that such an explanation is not correct.

A reasonable account for the different 10 Dq value measured in ruby and emerald has been obtained, however, through ab initio calculations on the simple CrO_6^{9-} complex (at the experimental equilibrium geometry) subject to the $V_R(\mathbf{r})$ potential corresponding to Al_2O_3 and $Be_3Si_6Al_2O_{18}$ lattices, respectively [18,19]. In such a case it was found $10\,\mathrm{Dq} = 18,180\,\mathrm{cm}^{-1}$ for $Al_2O_3 : Cr^{3+}$ while $10\,\mathrm{Dq} = 15,740\,\mathrm{cm}^{-1}$ for $Be_3Si_6Al_2O_{18} : Cr^{3+}$. These figures thus reasonably explain the $\sim 2,000\,\mathrm{cm}^{-1}$ difference between the ${}^4A_{2g} \rightarrow {}^4T_{2g}$ transition energies observed in ruby and emerald.

The quite different influence of $V_R(\mathbf{r})$ upon the final 10 Dq value in these lattices can be understood looking at Fig. 3 where the form of $V_R(\mathbf{r})$ along metal–ligand directions is portrayed. Although the D_3 local symmetry in emerald [6,40,42] avoids the existence of an electric field at the chromium site this is not longer true in the case of ruby as it is well shown

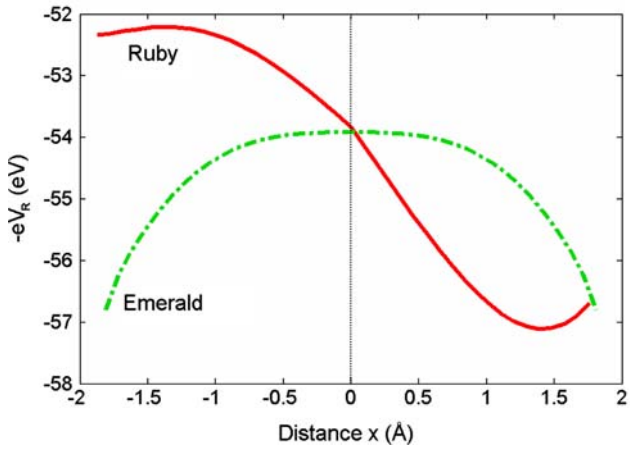

Fig. 3 Electrostatic potential, $V_R(x)$, of the rest of lattice ions on a CrO_6^{9-} complex along metal–ligand directions for ruby and emerald host lattices. For ruby $x > 0 (x < 0)$ corresponds to the long (short) bond with ligands at $R_l = 2.02$ Å ($R_s = 1.92$ Å) from chromium ion

in Fig. 3. For this reason, the value of Δ_R (defined in Eq. (2)) is found to be only equal to $-450\,\mathrm{cm}^{-1}$ for emerald while $\Delta_R = 2,100\,\mathrm{cm}^{-1}$ for ruby. A more detailed discussion on this issue is given in [18,19].

5 Final remarks

The present analysis shows that the distinct 10 Dq values exhibited by $KMgF_3 : Cr^{3+}$ and $BaLiF_3 : Cr^{3+}$ can hardly be ascribed mainly to the difference in the Cr^{3+}–F^- distance. By contrast, the main origin of this amazing fact can reasonably be assigned to the different $V_R(\mathbf{r})$ potential felt by active electrons in both types of cubic lattices. The present results thus stress the importance of this *internal electric field* when comparing the electronic properties of the same transition metal complex but embedded in two non-isomorphous lattices *even* if they are cubic. As emphasized in Sect. 4.2 the importance of $V_R(\mathbf{r})$ can grow when comparing the properties of the same impurity in two host lattices with the same ligand and coordination number but very different symmetry.

It should be remarked that the internal electric field, mainly felt by the electronic density placed around the ligands in $KMgF_3$ and $BaLiF_3$ host lattices, likely modifies the bonding properties of octahedral units like NiF_6^{4-}, MnF_6^{4-} or CrF_6^{3-} on passing from a normal to an inverted perovskite. A change of chemical bonding between the impurity and ligands due to $V_R(\mathbf{r})$ should also have some influence on the superhyperfine tensor and other optical and EPR parameters. A further study on this interesting issue is planned for a near future.

Acknowledgments Partial support by the Spanish Ministerio de Ciencia y Tecnología under Project FIS2006-02261 is acknowledged.

References

1. Jørgensen CK (1962) Absorption spectra and chemical bonding in complexes. Pergamon, Oxford
2. Sugano S, Tanabe Y, Kamimura H (1970) Multiplets of transition-metal ions in crystals. Academic, New York
3. Griffith JS (1961) The theory of transition-metal ions. Cambridge, Cambridge
4. Abragam A, Bleaney B (1970) Electron paramagnetic resonance of transition metal ions. London, Oxford
5. Lever AP (1984) Inorganic electronic spectroscopy, 2nd edn. Elsevier, Amsterdam
6. Burns RG (1993) Mineralogical applications of crystal field theory. Cambridge University Press, Cambridge
7. Moreno M, Barriuso MT, Aramburu JA, García-Fernandez P, García-Lastra JM (2006) J Phys Condens Matter 18:R315
8. Marco de Lucas M, Rodríguez F, Moreno M (1994) Phys Rev B 50:2760
9. Brik MG, Ogasawara K (2006) Phys Rev B 74:045105
10. Babel D, Tressaud A (1985) Inorganic solid fluorides, Hagenmuller P (ed), Academic, New York
11. Haussühl S, Leckebusch R, Recker K (1972) Z Naturf a 27:1022
12. Mortier M, Wang Q, Buzaré JY, Rousseau M, Piriou B (1997) Phys Rev B 56:3022
13. Mortier M, Gesland JY, Pirou B, Buzaré JY, Rousseau M (1994) Opt Mater 4:115
14. Yosida T (1980) J Phys Soc Japan 49:127
15. García-Lastra JM, Buzaré JY, Barriuso MT, Aramburu JA, Moreno M (2007) Phys Rev B 75:155101
16. Du Varney RC, Niklas JR, Spaeth JM (1981) Phys Stat Sol b 103:329
17. Aramburu JA, Paredes JI, Barriuso MT, Moreno M (2000) Phys Rev B 61:6525
18. García-Lastra JM, Barriuso MT, Aramburu JA, Moreno M (2005) Phys Rev B 72:113104
19. García-Lastra JM, Barriuso MT, Aramburu JA, Moreno M (2006) Phys Rev B 74:115118
20. Poole RT, Jenkin JG, Liesegang J, Leckey RCG (1975) Phys Rev B 11:5179
21. Fraga S, Karwowski J, Saxena KMS (1976) Handbook of atomic data. Elsevier, Amsterdam
22. Slater JC (1963) Quantum theory of molecules and solids (vol. 1). McGraw-Hill, New York
23. Kohn W (1968) Many body physics de Witt C, Balian R (ed), Gordon and Breach, New York
24. Aramburu JA, Moreno M, Cabria I, Barriuso MT, Sousa C, de Graaf C, Illas F (2000) Phys Rev B 62:13356
25. Sugano S, Shulman RG (1963) Phys Rev 130:517
26. Barandiarán Z, Pueyo L, Gómez Beltrán F (1983) J Chem Phys 78:4612
27. Barandiarán Z, Pueyo L (1983) J Chem Phys 79:1926
28. Barandiarán Z, Pueyo L (1983) J Chem Phys 80:1597
29. Pierloot K, Van Praet E, Vanquickenborne LG (1992) J Chem Phys 96:4163
30. Aramburu JA, Moreno M (1997) Phys Rev B 56:604
31. te Velde G, Bickelhaupt FM, van Gisbergen SJA, Fonseca Guerra C, Baerends EJ, Snijders JG, Ziegler T (2001) J Comput Chem 22:931–967
32. Barriuso MT, Aramburu JA, Moreno M (1999) J Phys Condens Matter 11:L525
33. Barriuso MT, Aramburu JA, Moreno M (2002) Phys Rev B 65:064441
34. Becke AD (1988) Phys Rev A 38:3098
35. Perdew JP (1986) Phys Rev B 33:8822
36. Piken AG, Van Gool W (1968) Technical report SL 68–10, Ford Motor Co. program modified by Aramburu JA (1996)

37. Atanasov M, Daul CA, Rauzy C (2003) Chem Phys Lett 367:737
38. Aramburu JA, Moreno M, Doclo K, Daul C, Barriuso MT (1999) J Chem Phys 110:1497
39. García-Fernandez P, García-Lastra JM, Aramburu JA, Barriuso MT, Moreno M (2006) Chem Phys Lett 426:91
40. Nassau K (1983) The physics and chemistry of colour. Wiley, New York
41. Powell RC (1998) Physics of solid-state laser materials. Springer, New York
42. Gaudry E (2004) Ph. D. Thesis, Université Paris 6
43. Gaudry E, Kiratisin A, Sainctavit P, Brouder C, Mauri F, Ramos A (2003) . Phys Rev B 67:094108
44. Gaudry E, Sainctavit P, Juillot F, Bondioli F, Ohresser Ph, Letard I (2006) Phys Chem Miner 32:710
45. Orgel LE (1957) Nature 179:1348